Applied Catalysis B: Environmental 117–118 (2012) 268–274

Contents lists available at SciVerse ScienceDirect

Applied Catalysis B: Environmental

journal homepage: www.elsevier.com/locate/apcatb

Synthesis of MWNTs/g-C_3N_4 composite photocatalysts with efficient visible light photocatalytic hydrogen evolution activity

Lei Ge [a,b,*], Changcun Han [b]

[a] State Key Laboratory of Heavy Oil Processing, China University of Petroleum Beijing, No. 18 Fuxue Rd., Beijing 102249, People's Republic of China
[b] Department of Materials Science and Engineering, College of Science, China University of Petroleum Beijing, No. 18 Fuxue Rd., Beijing 102249, People's Republic of China

ARTICLE INFO

Article history:
Received 6 November 2011
Received in revised form 6 January 2012
Accepted 19 January 2012
Available online 28 January 2012

Keywords:
Photocatalysis
Carbon nanotubes
Carbon nitrides
Hydrogen evolution

ABSTRACT

Novel multi-walled carbon nanotubes (MWNTs) and graphitic carbon nitride (g-C_3N_4) composite photocatalysts were synthesized via a facile heating method. The resulting MWNTs/g-C_3N_4 composite photocatalysts were characterized by X-ray diffraction (XRD), transmission electron microscopy (TEM), ultraviolet–visible diffuse reflection spectroscopy (DRS), X-ray photoelectron spectroscopy (XPS) and photoluminescence (PL) spectroscopy. The photoelectrochemical *I–t* curves were tested using several on–off cycles of visible light irradiation. The visible light photocatalytic hydrogen evolution was investigated for MWNTs/g-C_3N_4 in methanol aqueous solutions. The optimal MWNTs content is determined to be 2.0 wt%; and corresponding H_2 evolution rate is 7.58 μmol h^{-1}, about 3.7 folds that of pure g-C_3N_4. A possible mechanism of MWNTs on the enhancement of visible light performance is proposed. It suggests that MWNTs play key roles, which may lead to efficiently separation of the photo-generated charge carriers and, consequently, enhance the visible light photocatalytic H_2 production activity.

1. Introduction

The demand for clean energy technology has induced research in semiconductor photocatalysts for water splitting and environment purification [1–7]. Of particular interest is titanium dioxide (TiO_2) which is widely used as photocatalysts for the contaminant degradation and hydrogen generation [8–12]. However, only UV light (4% of the solar spectrum) can be used for TiO_2 photocatalytic reactions [13–16]. From the standpoint of solar energy availability, the exploitation of photocatalysts capable of photo-induced excitation in the visible light region is emerging as the important research trend in this field [17–20]. Recently, a variety of novel semiconductor photocatalysts such as doped titanium dioxide [21,22], multi-metal oxides [23–26], sulfides [27,28], oxynitrides [29,30], hetero structures [31,32] and polymers [33] have been successfully developed. These compounds exhibit activities in photocatalytic water splitting or pollutant degradation under visible light irradiation.

Polymeric graphitic carbon nitride (g-C_3N_4) has been a novel "metal-free" visible light induced semiconductor with narrow band gap energy of 2.7 eV [34]. Graphitic C_3N_4 has sufficient absorption and shows photocatalytic activity for hydrogen and oxygen evolution via water splitting within the solar spectrum [35–37]. Furthermore, it is inexpensive, environmentally benign, and can be easily prepared via numerous facile methods [38–40]. However, the photocatalytic efficiency of pure g-C_3N_4 is limited due to the recombination of its photo-generated electron-hole pairs. Very recently, several methods have been employed to improve the visible light photocatalytic activity of g-C_3N_4, for example, by preparing mesoporous structure [41], doping with metal or nonmetal species such as Fe [42], Ag [43], Au [37], S [44], B [45], and P [46], coupling utilizing TaON [47], Bi_2WO_6 [17], graphene [48], and sensitizing by organic dyes [49].

Ever since their discovery, the multi-walled carbon nanotubes (MWNTs) have received much interest for their special structures and unique electrical properties [50]. Moreover, MWNTs show higher electron conducting ability, which implies that they have potential applications in environmental field [51]. Recently, efforts have been devoted to synthesize MWNTs/TiO_2 composite, which show enhanced photocatalytic activity of pollutants degradation and water splitting [52,53]. Therefore, combining the polymeric g-C_3N_4 photocatalyst with the excellent charge transfer abilities of MWNTs, the obtained composite may be a promising candidate of efficient photocatalysts.

To the best of our knowledge, there are no reports on the synthesis and application of MWNTs/g-C_3N_4 composite for hydrogen evolution via photocatalytic water splitting. In this work, the novel MWNTs/g-C_3N_4 photocatalysts, which are composed of earth-abundant elements, were synthesized via a facile heating method.

* Corresponding author at: Department of Materials Science and Engineering, College of Science, China University of Petroleum Beijing, No. 18 Fuxue Rd., Beijing 102249, People's Republic of China. Tel.: +86 10 89733200.
E-mail address: gelei08@sina.com (L. Ge).

0926-3373/$ – see front matter © 2012 Elsevier B.V. All rights reserved.
doi:10.1016/j.apcatb.2012.01.021

The obtained composites show enhanced visible light photocatalytic activity than pure g-C_3N_4. The effect of MWNTs contents on the efficiency of photocatalytic hydrogen evolution is investigated and discussed in detail. A possible photocatalytic mechanism is also proposed.

2. Experimental

2.1. Synthesis of the photocatalyst

All chemicals were reagent grade and used without further purification. The multi-walled carbon nanotubes with high purities and 110 $m^2\,g^{-1}$ of surface area were purchased from the Cheap Tubes Inc., USA. The diameter of the MWNTs is 20–40 nm, and the length is 10–30 μm. Cyanamide was obtained from Aldrich.

The metal-free g-C_3N_4 powders were synthesized by heating 2.0 g of cyanamide in an alumina combustion boat under nitrogen gas flow (10 ml min^{-1}) to 550 °C at a heating rate of 10 °C min^{-1} followed by 4 h at that temperature prior to cooling. The product was collected and ground into a powder.

MWNTs/g-C_3N_4 composite photocatalysts were prepared as follows: cyanamide (2.0 g) was dispersed in distilled water (50 ml), and then the specified amount of MWNTs was added and ultrasonicated for 30 min to make MWNTs totally dispersed. After that, the product was collected and dried in an oven at 70 °C for 24 h. Finally, the resultant samples were heated to 550 °C for 4 h under N_2 gas flowing. The weight percentages of MWNTs in the composite photocatalysts were 0, 0.25, 0.5, 1.0, 2.0, 3.0 and 5.0, respectively.

2.2. Characterization

The crystal structure of the samples was investigated using X-ray diffraction (XRD; Bruker D8 Advance X-ray diffractometer) with Cu Kα radiation at a scan rate of 0.1° $2\theta\,s^{-1}$. The accelerating voltage and the applied current were 40 kV and 40 mA, respectively. The morphology of the samples was examined by transmission electron microscopy (TEM; FEI JEM-2100; accelerating voltage = 200 kV). UV–vis diffuse reflection spectroscopy (DRS) was performed on a Shimadzu UV-3101PC spectrophotometer using $BaSO_4$ as the reference. X-ray photoelectron spectroscopy (XPS) measurements were done on a Scienta R3000 XPS instrument with an Mg Kα source. The photoluminescence (PL) spectra of the photocatalyst were obtained by a Varian Cary Eclipse spectrometer with excitation wavelength of 325 nm.

2.3. Photocatalytic activity

The photocatalytic H_2 evolution experiments were performed in a 300 ml quartz reactor at ambient temperature. The reactor is connected to a closed circulating system. As light source, a PLS-SXE 300UV Xe arc lamp with a UV-cutoff filter (>400 nm) was used. In a typical photocatalytic experiment, 0.1 g of photocatalyst powder was suspended in 120 ml of aqueous solution containing 25% methanol by volume. The loading of 1.0 wt% Pt co-catalyst was conducted by directly dissolving H_2PtCl_6 into the mentioned suspension. Next, the suspensions were stirred and irradiated (300 W Xe arc lamp) for 30 min at room temperature to reduce the Pt species. Before photocatalytic experiments, the reaction vessel was evacuated for 30 min to remove the dissolved oxygen and to ensure the anaerobic conditions. The products were analyzed by gas chromatography (Shimadzu GC-8A, high purity argon as a carrier gas) equipped a thermal conductivity detector.

2.4. Photoelectrochemical measurements

Photocurrent measurements were performed on an electrochemical analyzer (Solartron SI 1287 Instruments) in a standard three-electrode configuration with a Pt wire as the counter electrode, and Ag/AgCl (in saturated KCl) as a reference electrode. Irradiation proceeded by a Xe arc lamp through a UV-cutoff filter (λ > 400 nm). Na_2SO_4 (0.01 M) aqueous solution was used as the electrolyte. The working electrodes were prepared as follows: the 0.05 g ground sample was mixed with 1 ml distilled water and 0.1 ml LIQUION solution was added to make slurry. The slurry was then injected onto a 2 cm × 0.5 cm FTO glass electrode and these electrolytes were dried at 120 °C for 30 min.

3. Results and discussion

3.1. Characterization of MWNTs/g-C_3N_4 composite samples

Fig. 1 shows the XRD patterns of the MWNTs/g-C_3N_4 samples of varying MWNTs contents with patterns for pure g-C_3N_4. All the samples have similar diffraction peaks. The pure g-C_3N_4 has two distinct diffraction peaks: the strong one at 27.40° represents the stacking of the conjugated double bonds, which is indexed for graphitic materials as the (0 0 2) peak and corresponding well to the interlayer d-spacing (0.336 nm) of g-C_3N_4. The diffraction peaks at 13.04°, corresponding to interplanar of 0.672 nm, are indexed as (1 0 0) in JCPDS 87-1526. These two diffraction peaks are in good agreement with the g-C_3N_4 reported in the literatures [34,48]. No diffraction peaks corresponding to MWNTs are observed in Fig. 1. This may be due to the small amount of MWNTs and highly dispersion in samples.

The morphology and microstructure of the MWNTs/g-C_3N_4 photocatalysts were investigated by TEM. Fig. 2 displays the TEM images of the pure g-C_3N_4 and MWNTs/g-C_3N_4 composite samples. As can be seen from Fig. 2a, the pure g-C_3N_4 sample consists of irregular particles with aggregated structures. Fig. 2b and c illustrates the microstructures of composite samples, the g-C_3N_4 particles bonded with MWNTs can be found, and the carbon nanotubes have different lengths and diameters, which indicate that the formation of interfaces between MWNTs and g-C_3N_4 particles.

The optical absorption of the as-prepared MWNTs/g-C_3N_4 composite samples was recorded using a UV–vis spectrometer and illustrated in Fig. 3. The pure g-C_3N_4 sample shows absorption from the UV through the visible range up to 460 nm, which can be ascribed to the band gap of g-C_3N_4 (2.7 eV) [34]. A comparison of the absorption spectra of the pure g-C_3N_4 with those acquired from the MWNTs/g-C_3N_4 composite samples shows that the

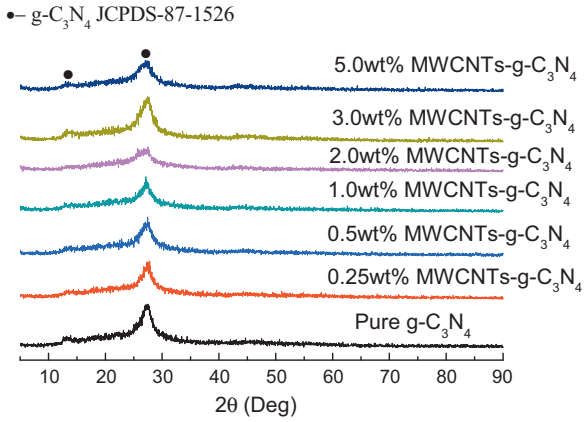

Fig. 1. XRD patterns of pure g-C_3N_4, as well as of the MWNTs/g-C_3N_4 composite photocatalysts.

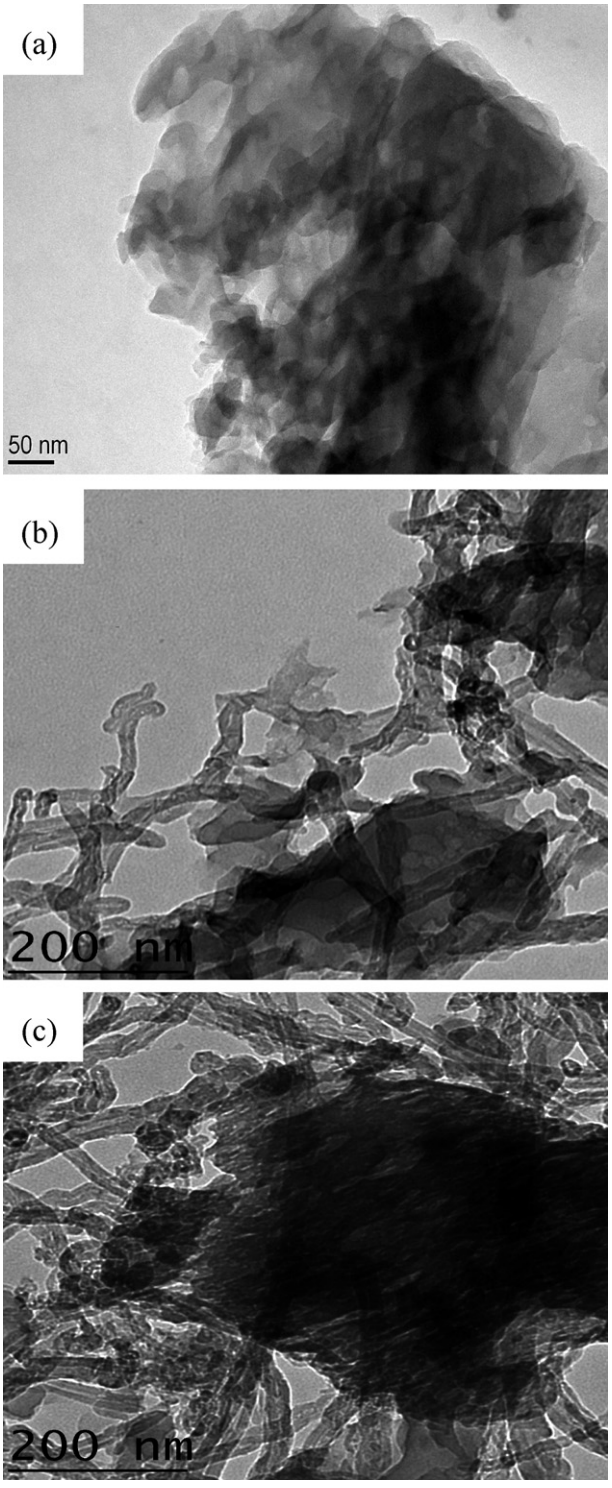

Fig. 2. TEM images of the composite samples: (a) pure g-C_3N_4; (b) 1.0 wt% MWNTs/g-C_3N_4; and (c) 2.0 wt% MWNTs/g-C_3N_4.

latter exhibit stronger absorption in the visible region at wavelengths longer than 400 nm, and the red shifts are also observed on the composite samples after addition of MWNTs. These experimental results can be attributed to the interaction between g-C_3N_4 and MWNTs in the composite samples. The absorption intensity of the as-prepared samples also strengthened with increasing MWNTs content (from 0 wt% to 5.0 wt%), which is in agreement with the color change from yellow to black. The absorption features suggest

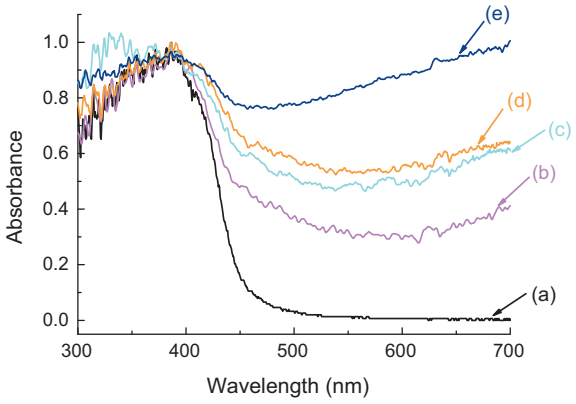

Fig. 3. UV–vis diffuse absorption spectra of MWNTs/g-C_3N_4 composite samples: (a) pure g-C_3N_4; (b) 1.0 wt% MWNTs/g-C_3N_4; (c) 2.0 wt% MWNTs/g-C_3N_4; (d) 3.0 wt% MWNTs/g-C_3N_4; and (e) 5.0 wt% MWNTs/g-C_3N_4. (For interpretation of the references to color in this figure legend, the reader is referred to the web version of the article.)

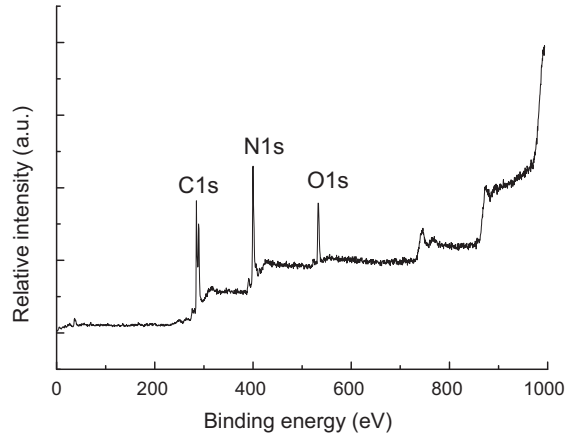

Fig. 4. XPS survey spectrum of the 2.0 wt% MWNTs/g-C_3N_4.

that the prepared MWNTs/g-C_3N_4 photocatalyst should be responsive to the visible-light.

X-ray photoelectron spectrum is used to investigate the valance states and chemical environment of constituent elements on the surface of sample. The sample for XPS is 2.0 wt% MWNTs/g-C_3N_4. The survey XPS spectrum (Fig. 4) shows that the main elements on the surface of the product are C, N and small amount of adsorbed O. The photoelectron peaks appear at binding energies of 285 eV (C 1s), 400.1 eV (N 1s), and 532.6 eV (O 1s).

Fig. 5a shows the high resolution C 1s XPS spectra of the 2.0 wt% MWNTs/g-C_3N_4 composite sample: the C 1s photoelectron signal has two distinct peaks at 285.13 and 288.27 eV. The XPS peak with binding energy of 285.13 is attributed to graphitic carbon adsorbed to the surface and C—C bond from MWNTs [48], which indicate the formation of interaction between MWNTs and g-C3N4. In contrast, the XPS peak at 288.27 eV originates from carbon atoms bonded to three nitrogen atoms in the g-C3N4 lattice [33]. The high resolution N 1s XPS spectra (Fig. 5b) show an asymmetrical feature indicating the co-existence of a number of distinguishable nitrogen environments; fitting with three results in binding energies of 398.6, 399.8 and 401.5 eV. The two peaks at 399.8 and 401.5 eV can be assigned to tertiary nitrogen (N—$(C)_3$) and amino functional groups having a hydrogen atom (C—N—H) [48,53]. The peak at 398.6 eV is typically attributed to N atoms sp^2-bonded to two carbon atoms (C=N—C) [33], thus confirming the presence of graphite-like sp^2-bonded graphitic carbon nitride.

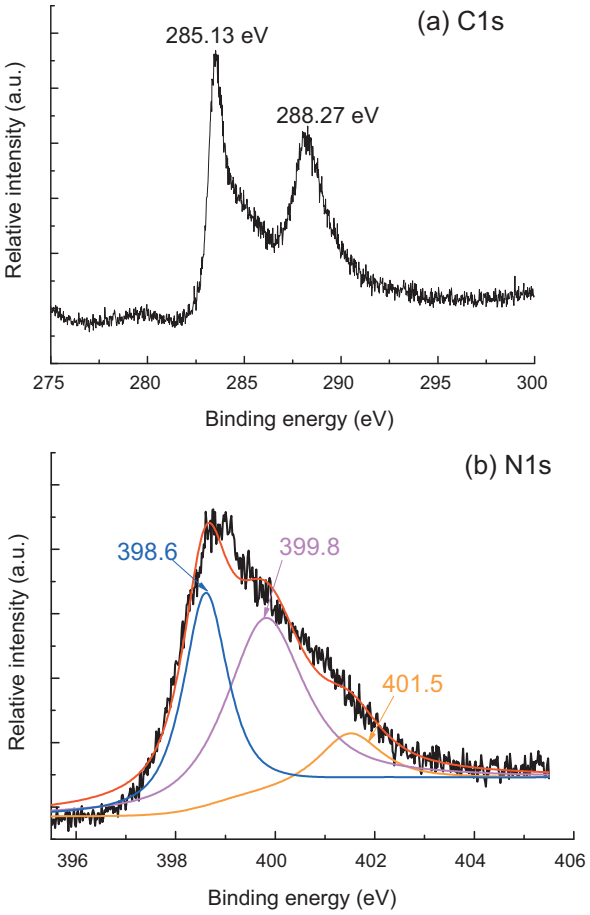

Fig. 5. High-resolution XPS spectra of C 1s for the 2.0 wt% MWNTs/g-C_3N_4: (a) C 1s; and (b) N 1s.

3.2. Photocatalytic H_2 evolution

The photocatalytic activity of the composite photocatalyst was evaluated by hydrogen evolution over different samples loaded with 1.0 wt% Pt in aqueous methanol solution under visible light irradiation (>400 nm). Fig. 6 shows the H_2 evolution rate over samples with different MWNTs loading contents under visible light irradiation.

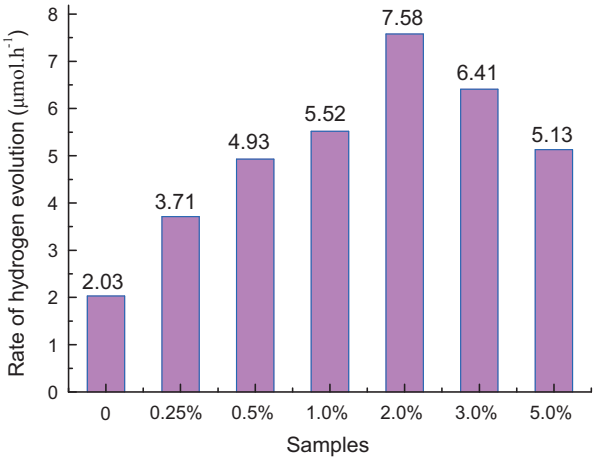

Fig. 6. Photocatalytic H_2 evolution over the MWNTs/g-C_3N_4 composite samples from methanol aqueous solution under visible light irradiation ($\lambda > 400$ nm).

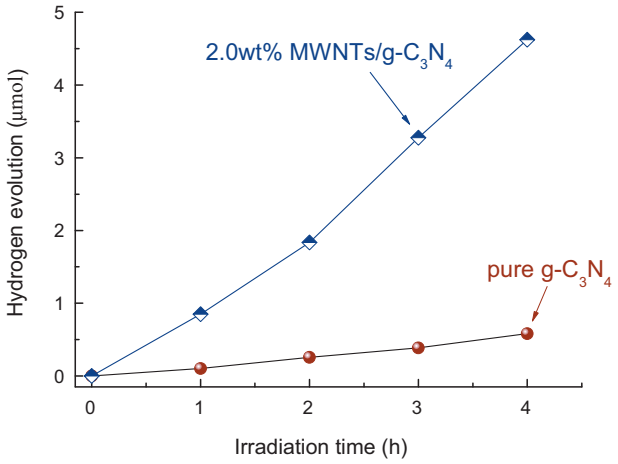

Fig. 7. Photocatalytic H_2 evolution over the 2.0 wt% MWNTs/g-C_3N_4 and pure g-C_3N_4 samples without adding Pt co-catalysts.

As can be seen from Fig. 6, pure g-C_3N_4 sample shows obvious visible light photocatalytic activity with H_2 evolution rate of 2.03 μmol h^{-1}, which can be attributed to the moderate band gap and unique electronic structure of g-C_3N_4. After addition of a small amount of MWNTs, the photocatalytic activity of 0.25 wt% MWNTs/g-C_3N_4 sample is improved. The activity of the composite samples is further enhanced with higher MWNTs content from 0.25 wt% to 2.0 wt%. The 2.0 wt% MWNTs/g-C_3N_4 sample shows the highest H_2 evolution rate of 7.58 μmol h^{-1}, which is about 3.7 folds higher than that of pure g-C_3N_4. Fig. 6 emphasizes that the MWNTs content is pivotal for optimal photocatalytic activity: when the MWNTs content is higher than 2.0 wt%, a further increase in MWNTs content causes a decrease in the photocatalytic H_2 evolution. We propose that the origin of this effect is attributed to the increase in the opacity and light scattering at higher MWNTs contents, leading to decrease of light passing through the reaction suspension solution. A similar observation has been reported previously for MWNTs/TiO_2 composites [54].

To confirm the role of MWNTs as a hydrogen evolution site, the photocatalytic experiments without adding Pt co-catalysts were performed and illustrated in Fig. 7. As shown in this figure, the H_2 production rate of 1.15 μmol h^{-1} is observed over the 2.0 wt% MWNTs/g-C_3N_4 samples, and the hydrogen evolution activities are much lower than the samples with Pt co-catalysts. However, the photocatalytic activity of pure g-C_3N_4 photocatalyst is only 0.146 μmol h^{-1}, which indicate that the MWNTs play an important role in enhancement of hydrogen evolution activity in the MWNTs/g-C_3N_4 photocatalysts.

Besides activity, the stability of a photocatalyst is important for application. To demonstrate the stability of our composite catalysts, we performed the cycled the hydrogen evolution experiment over 2.0 wt% samples under the same conditions. Fig. 8 displays the H_2 evolution curve in cycling photocatalytic run. No obvious decrease of H_2 evolution is observed after irradiated for 28 h. In many cases where the nitrogen-containing materials are used as photocatalysts, a low level of N_2 is detected in the photocatalytic reaction [34]. To further confirm the stability of the MWNTs/g-C_3N_4 photocatalyst, the N_2 evolution in the photocatalytic experiments was used to evaluate the stability of MWNTs/g-C_3N_4 photocatalysts. No N_2 evolution is observed for the composite photocatalysts under visible light irradiation. The XRD patterns were also performed to determine the structure variations of the composite samples and shown in Fig. 9. The results reveal that the crystal structures of the MWNTs/g-C_3N_4 photocatalysts do not change after the

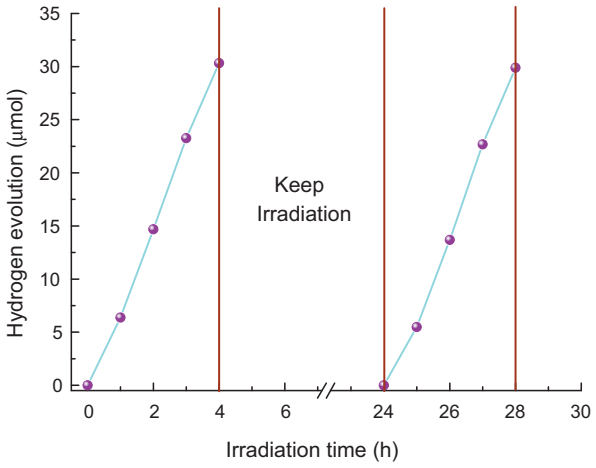

Fig. 8. Cycling runs for the photocatalytic H_2 evolution in the presence of 2.0 wt% MWNTs/g-C_3N_4 composite under visible light irradiation.

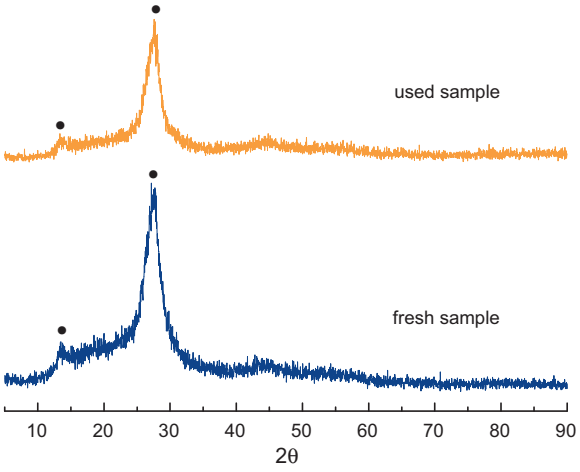

Fig. 9. XRD patterns of 2.0 wt% MWNTs/g-C_3N_4 before and after the cycling photocatalytic experiments.

photocatalytic reaction. These results indicate excellent stability of the MWNTs/g-C_3N_4 samples for photocatalytic H_2 evolution.

Based on the results of structure characterizations and the visible light photocatalytic tests of the as-prepared samples, a possible mechanism for photocatalytic H_2 evolution on MWNTs/g-C_3N_4 catalyst is proposed and illustrated in Fig. 10. The significant enhancement of H_2 evolution can be attributed to synergistic effect between g-C_3N_4 and MWNTs. After the MWNTs are introduced, the two types of materials closely combine together and form interfaces. The MWNTs can act as effective electron transfer channel since they possess high electrical conductivity and high electron storage capacity [50,51]. MWNTs have higher capture electron capability and can stimulate electron transfer from g-C_3N_4 towards MWNTs surface due to the lower Fermi level. Thus the Schottky barrier forms at the interface between the g-C_3N_4 and MWNTs. As can be seen from Fig. 10, the polymeric g-C_3N_4 in the composite photocatalyst absorbs photons as well as excites electron and hole pairs when the system is irradiated with visible light. The photogenerated electrons in the conduction band (CB) of g-C_3N_4 tend to immigrate towards the MWNTs surface, while the holes remain in valance band (VB). The electrons transferred from g-C_3N_4 will accumulate on the surface of MWNTs and Pt nanoparticles, and then participate in H_2 evolution. And the holes at the VB can react with methanol as a sacrificial reagent. Therefore, the

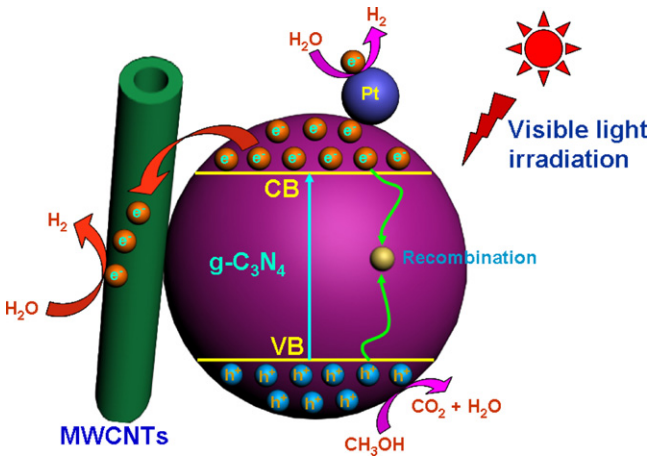

Fig. 10. Schematic of photo-generated charge carrier's separation and transfer in the MWNTs/g-C_3N_4 system under visible light irradiation.

efficient electron–hole separation leads to significant enhancement of photocatalytic H_2 evolution in the MWNTs/g-C_3N_4 composite system.

To verify the photocatalytic mechanism, the 2.0 wt% MWNTs/g-C_3N_4 samples after photocatalytic reactions were analyzed by SEM and TEM. As can be seen from Fig. 11, the Pt particles are found on the MWNTs surface, which indicates that the photogenerated

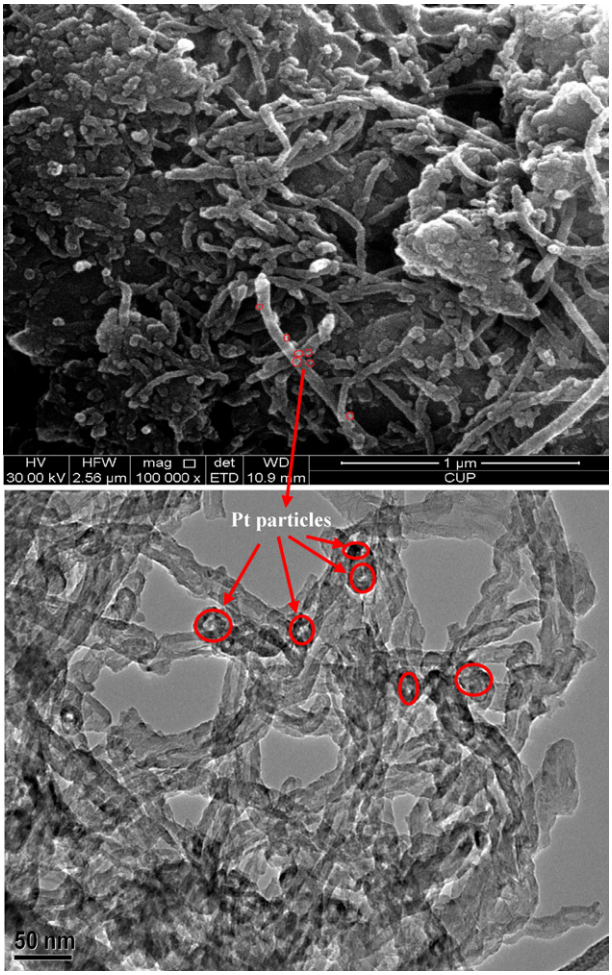

Fig. 11. SEM and TEM micrographs of 2.0 wt% MWNTs/g-C_3N_4 samples after photocatalytic reactions.

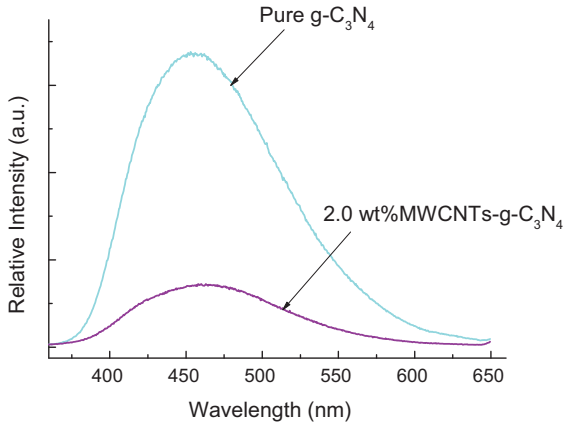

Fig. 12. Comparison of photoluminescence (PL) spectra of pure g-C_3N_4 and MWNTs/g-C_3N_4 samples.

electrons may transfer from g-C_3N_4 towards MWNTs surface and then reduce Pt species. The experiment results are consistent with the mechanism illustrated in Fig. 10.

In order to investigate the effect of the MWNTs modification, photoluminescence spectra analysis was applied to reveal the migration, transfer and recombination processes of photogenerated electron–hole pairs in composite samples. Fig. 12 presents the PL spectra for pure g-C_3N_4 and 2.0 wt% MWNTs/g-C_3N_4 with an excitation wavelength of 325 nm. As shown in Fig. 12, the main emission peak is centered at about 460 nm for the pure g-C_3N_4 sample, which can be attributed to the band–band PL phenomenon with the energy of light approximately equal to the band gap energy of g-C_3N_4 [48]. The emission intensity of PL spectrum for the MWNTs/g-C_3N_4 composite photocatalysts significantly decreases, which indicates that the composite has a much lower recombination rate of photo-generated charge carriers.

The transient photocurrent responses of the pure g-C_3N_4 and 2.0 wt% MWNTs/g-C_3N_4 samples were investigated for several on–off cycles of irradiation to give further evidence to support the proposed photocatalytic mechanism. Fig. 13 shows a plot of photocurrent density versus the irradiation time for as-prepared samples with chopped illumination. The photocurrent densities rapidly decrease to zero as soon as the lamp turns off, and the photocurrent comes back to stable values when the lamp is turned on. This phenomenon indicates that the photogenerated electrons migrate to the ITO substrates to produce photocurrent under visible light irradiation [55]. As shown in Fig. 13, the MWNTs/g-C_3N_4 composite photocatalyst shows higher photocurrent intensity than that

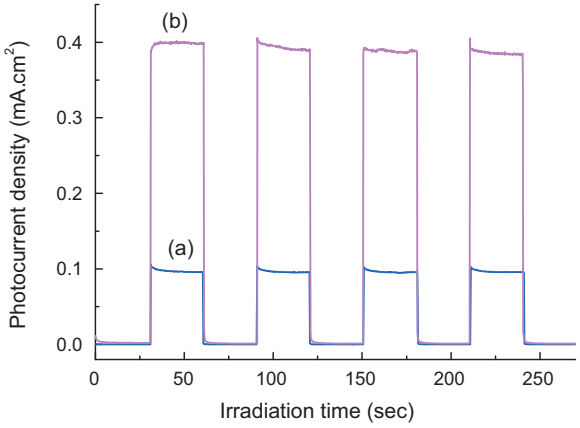

Fig. 13. Transient photocurrent response for the (a) pure g-C_3N_4 samples; and (b) 2.0 wt% MWNTs/g-C_3N_4.

of pure g-C_3N_4. The photoelectrochemical result also demonstrates a lower rate of recombination and more efficient separation of photogenerated electron–hole pairs for the MWNTs/g-C_3N_4 composite samples at the interface between MWNTs and g-C_3N_4. Therefore, the PL spectra and photoelectrochemical result confirm with the discussion on the charge carrier separation and photocatalytic experiments.

4. Conclusions

Novel MWNTs/g-C_3N_4 composite photocatalysts were successfully prepared via facile heating method. The structure, surface morphology and element chemical states have been investigated. The interfaces between MWNTs and g-C_3N_4 are clearly found in the composite samples. The MWNTs/g-C_3N_4 composites have strong absorption in the visible light region. After introduction of MWNTs, the g-C_3N_4 photocatalysts show significant enhancement of the visible light photocatalytic activity. The optimal MWNTs content is determined to be 2.0 wt% with H_2 evolution rate of 7.58 μmol h^{-1}, which is about 3.7 folds than that of pure g-C_3N_4. A possible photocatalytic mechanism is proposed based on the experimental results. The MWNTs have higher capture electron capability and can promote electron transfer from g-C_3N_4 towards their surface, leading to the improvement of photocatalytic performance.

Acknowledgments

This work was financially supported by the National Science Foundation of China (grant no. 21003157), Beijing Nova Program (grant no. 2008B76) and Doctor Foundation of Chinese Ministry of Education (grant no. 200804251014).

References

[1] X.B. Chen, S.H. Shen, L.J. Guo, A.S. Mao, Chem. Rev. 110 (2010) 6503–6570.
[2] H. Zhang, Y.F. Zhu, J. Phys. Chem. C 114 (2010) 5822–5826.
[3] X.F. Wang, Y.H. Shen, A.J. Xie, A.G. Qiu, S.K. Li, Y. Wang, J. Mater. Chem. 21 (2011) 9641–9646.
[4] E.P. Gao, W.Z. Wang, M. Shang, J.H. Xu, Phys. Chem. Chem. Phys. 13 (2011) 2887–2893.
[5] L. Ge, J. Liu, Appl. Catal. B: Environ. 105 (2011) 289–297.
[6] A. Kudo, Y. Miseki, Chem. Soc. Rev. 38 (2009) 253–278.
[7] L. Ge, M.X. Xu, H.B. Fang, Mater. Lett. 61 (2007) 63–66.
[8] X. Yang, C. Cao, L. Erickson, K. Hohn, R. Maghirang, K. Klabunde, Appl. Catal. B: Environ. 91 (2009) 657–662.
[9] C. Han, M. Pelaez, V. Likodimos, A.G. Kontos, P. Falaras, K. O'Shea, D. Dionysiou, Appl. Catal. B: Environ. 107 (2011) 77–87.
[10] D.B. Hamal, K.J. Klabunde, J. Phys. Chem. C 115 (2011) 17359–17367.
[11] L. Ge, M.X. Xu, H.B. Fang, Thin Solid Films 515 (2007) 3414–3420.
[12] H.Q. Lu, J.H. Zhao, L. Li, L.M. Gong, J.F. Zhang, L.X. Zhang, Z.J. Wang, J. Zhang, Z.P. Zhu, Energy Environ. Sci. 4 (2011) 3384–3388.
[13] G.B. Soares, B. Bravin, C.M.P. Vaz, C. Ribeiro, Appl. Catal. B: Environ. 106 (2011) 287–294.
[14] M.I. Mejia, J.M. Marin, G. Restrepo, L.A. Rios, C. Pulgarin, J. Kiwi, Appl. Catal. B: Environ. 94 (2010) 166–172.
[15] Y. Yalcin, M. Kilic, Z. Cinar, Appl. Catal. B: Environ. 99 (2010) 469–477.
[16] X.B. Chen, L. Liu, P.Y. Yu, S.S. Mao, Science 331 (2011) 746–750.
[17] L. Ge, C.C. Han, J. Liu, Appl. Catal. B: Environ. 108 (2011) 100–107.
[18] S.J. Hong, S. Lee, J.S. Jang, J.S. Lee, Energy Environ. Sci. 4 (2011) 1781–1787.
[19] L. Ge, J. Mol. Catal. A: Chem. 282 (2008) 62–66.
[20] J.L. Gunjakar, T.W. Kim, H.N. Kim, I.Y. Kim, S.J. Hwang, J. Am. Chem. Soc. 133 (2011) 14998–15007.
[21] H.N. Kim, T.W. Kim, I.Y. Kim, S.J. Hwang, Adv. Funct. Mater. 21 (2011) 3111–3118.
[22] V.B.R. Boppana, R.F. Lobo, J. Catal. 281 (2011) 156–168.
[23] Z.G. Yi, J.H. Ye, N. Kikugawa, T. Kako, S.X. Ouyang, H.S. William, H. Yang, J.Y. Cao, W.J. Luo, Z.S. Li, Y. Liu, R.L. Withers, Nat. Mater. 9 (2010) 559–564.
[24] B. Zhou, X. Zhao, H.J. Liu, J.H. Qu, C.P. Huang, Appl. Catal. B: Environ. 99 (2010) 214–221.
[25] J.H. Ye, Z.G. Zou, A. Matsushita, Int. J. Hydrogen Energy 28 (2003) 651–655.
[26] L. Ge, Mater. Chem. Phys. 107 (2008) 465–470.
[27] Q. Li, B.D. Guo, J.G. Yu, J.R. Ran, B.H. Zhang, H.J. Yan, J.R. Gong, J. Am. Chem. Soc. 133 (2011) 10878–10884.
[28] X. Zong, G.P. Wu, H.J. Yan, G.J. Ma, J.Y. Shi, F.Y. Wen, L. Wang, C. Li, J. Phys. Chem C 114 (2010) 1963–1968.

[29] K. Maeda, K. Domen, MRS Bull. 36 (2011) 25–31.
[30] K. Maeda, M. Higashi, B. Siritanaratkul, R. Abe, K. Domen, J. Am. Chem. Soc. 133 (2011) 12334–12337.
[31] J. Su, X.X. Zou, G.D. Li, X. Wei, C. Yan, Y.N. Wang, J. Zhao, L.J. Zhou, J.S. Chen, J. Phys. Chem. C 115 (2011) 8064–8071.
[32] L. Ge, J. Liu, Mater. Lett. 65 (2011) 1828–1831.
[33] A. Thomas, A. Fischer, F. Goettmann, M. Antonietti, J.O. Müller, R. Schlogl, J.M. Carlsson, J. Mater. Chem. 18 (2008) 4893–4908.
[34] X.C. Wang, K. Maeda, A. Thomas, K. Takanabe, G. Xin, J.M. Carlsson, K. Domen, M. Antonietti, Nat. Mater. 8 (2009) 76–80.
[35] K. Maeda, X.C. Wang, Y. Nishihara, D.L. Lu, M. Antonietti, K. Domen, J. Phys. Chem. C 113 (2009) 4940–4947.
[36] X.C. Wang, K. Maeda, X.F. Chen, K. Takanabe, K. Domen, Y.D. Hou, X.Z. Fu, M. Antonietti, J. Am. Chem. Soc. 131 (2009) 1680–1681.
[37] Y. Di, X.C. Wang, A. Thomas, A. Antonietti, ChemCatChem 2 (2010) 834–838.
[38] F. Dong, L.W. Wu, Y.J. Sun, M. Fu, Z.B. Wu, S.C. Lee, J. Mater. Chem. 21 (2011) 15171–15174.
[39] Y. Wang, X.C. Wang, M. Antonietti, Y.J. Zhang, ChemSusChem 3 (2010) 435–439.
[40] S.C. Yan, Z.S. Li, Z.G. Zou, Langmuir 25 (2009) 10397–10401.
[41] F.Z. Su, S.C. Mathew, G. Lipner, X.Z. Fu, M. Antonietti, J. Am. Chem. Soc. 132 (2010) 16299–16301.
[42] X.F. Chen, J.S. Zhang, X.Z. Fu, M. Antonietti, X.C. Wang, J. Am. Chem. Soc. 131 (2009) 11658–11659.
[43] L. Ge, C.C. Han, J. Liu, Y.F. Li, Appl. Catal. A: Gen. 409–410 (2011) 215–222.
[44] G. Liu, P. Niu, C. Sun, S.C. Smith, Z. Chen, G.Q. Lu, H.M. Cheng, J. Am. Chem. Soc. 132 (2010) 11642–11648.
[45] S.C. Yan, Z.S. Li, Z.G. Zou, Langmuir 26 (2010) 3894–3901.
[46] Y.J. Zhang, T. Mori, J.H. Ye, M. Antonietti, J. Am. Chem. Soc. 132 (2010) 6294–6295.
[47] S.C. Yan, S.B. Lv, Z.S. Li, Z.G. Zou, Dalton Trans. 39 (2010) 1488–1491.
[48] Q.J. Xiang, J.G. Yu, M. Jaroniec, J. Phys. Chem. C 115 (2011) 7355–7363.
[49] H.J. Yan, H. Yan, Chem. Commun. 47 (2011) 4168–4170.
[50] Y. Cong, X.K. Li, Y. Qin, Z.J. Dong, G.M. Yuan, Z.W. Cui, X.J. Lai, Appl. Catal. B: Environ. 107 (2011) 128–134.
[51] O. Akhavan, M. Abdolahad, Y. Abdi, S. Mohajerzadeh, Carbon 47 (2009) 3280–3287.
[52] K. Dai, T.Y. Peng, D.N. Ke, B.Q. Wei, Nanotechnology 20 (2009) 125603.
[53] Y.Q. Sun, C. Liu, Y.X. Xu, H. Bai, Z.Y. Yao, G.Q. Shi, Chem. Commun. 46 (2010) 4740–4742.
[54] C.Y. Yen, Y.F. Lin, C.H. Hung, Y.H. Tseng, C.C. Ma, M.C. Chang, H. Shao, Nanotechnology 19 (2008) 045604.
[55] J.G. Yu, G.P. Dai, B. Cheng, J. Phys. Chem. C 114 (2010) 19378–19385.